Inlet Measurements and Quiet Flow Improvements in the Boeing/AFOSR Mach-6 Quiet Tunnel

AIAA Paper 2006-1317, presented at the 44th AIAA Aerospace Sciences Meeting, Reno, NV, Jan. 2006

Matthew P. Borg*, Steven P. Schneider†, and Thomas J. Juliano‡
School of Aeronautics and Astronautics
Purdue University
West Lafayette, IN 47907-1282

Abstract

The Boeing/AFOSR Mach-6 Quiet Tunnel (BAM6QT) has been developed to provide quiet flow at high Reynolds number, with low noise levels comparable to flight. Laminar nozzle-wall boundary layers and the resulting quiet flow have now been achieved to moderately high Reynolds numbers of 2.1×10^6/ft., after four years of shakedown. The BAM6QT is now the only operational hypersonic quiet tunnel, anywhere.

Problems with early transition were apparently due to a small flaw in the leading edge of the bleed lip of the original electroformed-nickel throat. The bleed lips of the nickel throat and the new aluminum surrogate throat are now being modified to eliminate separation bubbles that are still predicted by Rutgers-University computations.

The flow in the inlet to the contraction was also examined in order to determine the level of disturbances present there. A new hot-wire calibration technique was developed that is suitable for the incompressible yet varying density flow present in the contraction. The noise levels were asymmetric but typically on the order of 1%. There is also evidence of a highly asymmetric boundary layer in the contraction. These asymmetries are thought to be caused by pre-run free convection in the contraction.

*Research Assistant. Student Member, AIAA.
†Professor. Associate Fellow, AIAA.
‡Research Assistant. Student Member, AIAA.

Introduction

Hypersonic Laminar-Turbulent Transition

Laminar-turbulent transition in hypersonic boundary layers is important for prediction and control of heat transfer, skin friction, and other boundary layer properties. Vehicles that spend extended periods at hypersonic speeds may be critically affected by the uncertainties in transition prediction, depending on their Reynolds numbers. Although slender vehicles are the primary concern, blunt vehicles are also affected by transition [1]. However, the mechanisms leading to transition are still poorly understood, even in low-noise environments.

Many transition experiments have been carried out in conventional ground-testing facilities over the past 50 years [2]. However, these experiments are contaminated by the high levels of noise that radiate from the turbulent boundary layers normally present on the wind tunnel walls [3]. These noise levels, typically 0.5-1% of the mean, are an order of magnitude larger than those observed in flight [4, 5]. These high noise levels can cause transition to occur an order of magnitude earlier than in flight [3, 5]. In addition, the mechanisms of transition operational in small-disturbance environments can be changed or bypassed altogether in high-noise environments; these changes in the mechanisms change the parametric trends in transition [4]. Mechanism-based prediction methods must be developed, supported in part with measurements of the mechanisms in quiet wind tunnels.

Development of Quiet-Flow Wind Tunnels

Only in the last two decades have low-noise supersonic wind tunnels been developed [3, 6]. This development has been difficult, since the test-section wall boundary-layers must be kept laminar in order

to avoid high levels of eddy-Mach-wave acoustic radiation from the normally-present turbulent boundary layers. A Mach-3.5 tunnel was the first to be successfully developed at NASA Langley [7]. Langley then developed a Mach-6 quiet nozzle, which was used as a starting point for the new Purdue nozzle [8]. Unfortunately, this nozzle was removed from service due to a space conflict; it is now to be reinstalled at Texas A&M. The Purdue Mach-6 tunnel is presently the only operational hypersonic quiet tunnel, anywhere in the world.

Background of the Boeing/AFOSR Mach-6 Quiet Tunnel

A Mach-4 Ludwieg tube was developed at Purdue in 1992-1994 [9]. Quiet flow was achieved at low Reynolds numbers, and the facility was used for development of instrumentation and for measurements of instability waves under quiet-flow conditions. However, the low quiet Reynolds number and the small 4-inch test section imposed severe limitations.

A hypersonic facility that remained quiet to higher Reynolds numbers was needed. Low operating costs had to be maintained, to make research affordable in the post-Cold-War environment. Beginning with Ref. [10], a series of AIAA papers have reported on the design, fabrication, and shakedown of this facility, on the development of instrumentation, and on progress towards achieving Mach-6 quiet flow at high Reynolds number. Refs. [11] and [12] summarize these earlier papers, including the initial quiet flow achieved at low Reynolds numbers (8 psia stagnation pressure) with the 6th bleed-slot design. Ref. [13] reported initial achievement of quiet flow at 20 psia stagnation pressure, using the unpolished surrogate throat. Ref. [14] reported hot-wire measurements of second-mode instabilities on sharp and blunt cones at conventional-noise conditions.

The present paper reports progress in the second half of 2005. Quiet flow was recently achieved at high Reynolds number for the first time. Recent computations show that a separation bubble is forming on the main-flow side of the bleed lip [15, 16]; at present, this appears to remain the probable cause of transition in the nozzle-wall boundary layer.

The Boeing/AFOSR Mach-6 Quiet Tunnel

Quiet facilities require low levels of noise in the inviscid flow entering the nozzle through the throat, and laminar boundary layers on the nozzle walls. To reach these low noise levels, conventional blow-down facilities must be extensively modified. Requirements include a 1 micron particle filter, a highly polished nozzle with bleed slots for the contraction-wall boundary layer, and a large settling chamber with screens and sintered-mesh plates for noise-reduction [3]. To reach these low noise levels in an affordable way, the Purdue facility has been designed as a Ludwieg tube [9]. A Ludwieg tube is a long pipe with a converging-diverging nozzle on the end, from which flow exits into the nozzle, test section, and second throat (Figure 1). Care is taken to keep the air in the tunnel as dry as possible to avoid water condensation in the nozzle. The dewpoint of the air in the tunnel, measured with a Panametrics Moisture Target Series-5 dewpoint meter, was typically on the order of $-20°$C.

A diaphragm is placed downstream of the test section. When the diaphragm bursts, an expansion wave travels upstream through the test section into the driver tube. Since the flow remains quiet after the wave reflects from the contraction, sufficient vacuum can extend the useful runtime to many cycles of expansion-wave reflection, during which the pressure drops quasi-statically.

The contraction-wall boundary layer is bled off just upstream of the throat, beginning a fresh undisturbed boundary layer for the nozzle wall. The nozzle-throat bleed air can be ducted to two alternate locations. A fast valve remains connected directly between the bleeds and the vacuum tank, allowing the bleed air to be dumped directly into the tank, with a small but significant delay of about 1/2 sec., which increases to perhaps 2 sec. at very low pressures, where the existing valve does not work well. In addition, the original plumbing connecting the bleed air to the diffuser enables a faster startup, if the jets of air into the diffuser are not a problem.

Figure 2 shows the nozzle. Here, z is an axial coordinate whose origin is at the nozzle throat. The region of useful quiet flow lies between the characteristics marking the onset of uniform flow, and the characteristics marking the upstream boundary of acoustic radiation from the onset of turbulence in the nozzle-wall boundary layer. A 7.5-deg. sharp cone is drawn on the figure. The rectangles are drawn on the nozzle at the location of window openings, all but one of which are presently filled with blank metal inserts. Images of the tunnel are available at `http://roger.ecn.purdue.edu/~aae519/BAM6QT-Mach-6-tunnel/`, along with earlier papers and other documentation.

Quiet Flow Achieved to High Reynolds Number

Quiet flow at high Reynolds number was recently achieved for the first time in the Boeing/AFOSR

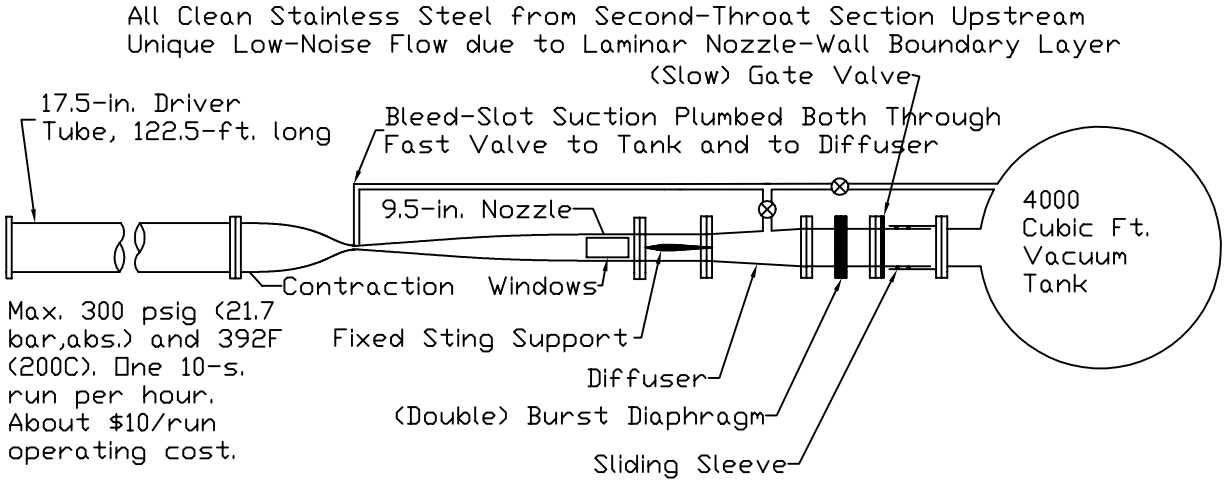

Figure 1: Schematic of Boeing/AFOSR Mach-6 Quiet Tunnel

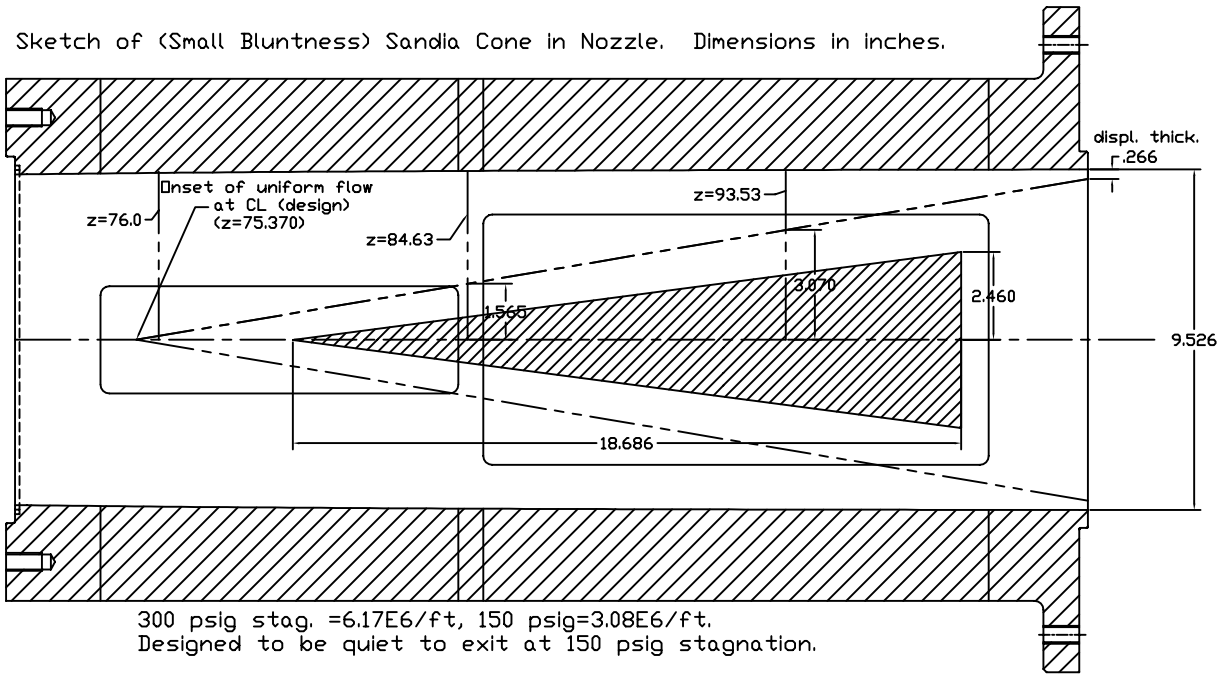

Figure 2: Schematic of Mach-6 Quiet Nozzle with Model

Mach-6 Quiet Tunnel at Purdue. All the measurements were performed at a stagnation temperature of 160°C.

Initial Tests with Surrogate Throat

An aluminum surrogate throat was machined in sections in Spring 2005 [13]. The purpose was to develop a low-cost throat that could be instrumented without risk to the highly polished joint-free electroformed-nickel throat. At best, the surrogate throat was expected to perform similarly to the nickel throat, since the sectioning added roughness at the joints, and the soft aluminum cannot be polished as well as the harder nickel.

Surprisingly, the first tests with the surrogate throat achieved quiet flow up to 20 psia [13]. When the throat was removed, an aft-facing step was noted at the end of the surrogate throat, at $z = 30.265$. Here, z is the axial distance downstream from the throat. This step was only about 0.002 inches high, as estimated by Mr. Jerry Hahn in the AAE machine shop. This is only about half the allowable roughness according to the $Re_k = 12$ criterion, even at 150 psia stagnation pressure (Fig. 41 of Ref. [10]). However, it was still decided to reduce the step, just to see what would happen, and because it was not difficult. Mr. Jerry Hahn of the AAE machine shop increased the inner diameter of 5.5686 in. to 5.5730 in. at $z = 30.2650$ in., starting the new profile at $z = 23.675$ at 4.605-in. dia., and cutting in a straight line to 5.573-in. dia. Thus, the inside diameter at the end of the surrogate throat was increased by 0.0044 inches, making it nearly flush at the joint with section 5, although not as flush as the original nickel throat, which was hand-polished as an assembly.

The modified surrogate nozzle was then tested using centerline pitot measurements near the nozzle exit. Surprisingly, again, the flow became quiet at a much higher stagnation pressure, about 37 psia. It seems likely that small streamwise vortices generated at the aft-facing step must have been feeding the Görtler instability, which should begin near the beginning of the concave-wall region, at $z = 23.668$ in. (38.31 throat radii per Table 1 of Ref. [10]). Since the end of the throat section at $z = 30.265$ in. is just downstream of the beginning of the concave-curvature region in this very long nozzle with a 4-deg. inflection angle, small vortices generated from the step are well positioned to amplify.

Bleed-Lip Separation and Tip Flaws

These results with the surrogate nozzle showed clearly that the longstanding early nozzle-wall transition was caused by some flaw in the nickel throat.

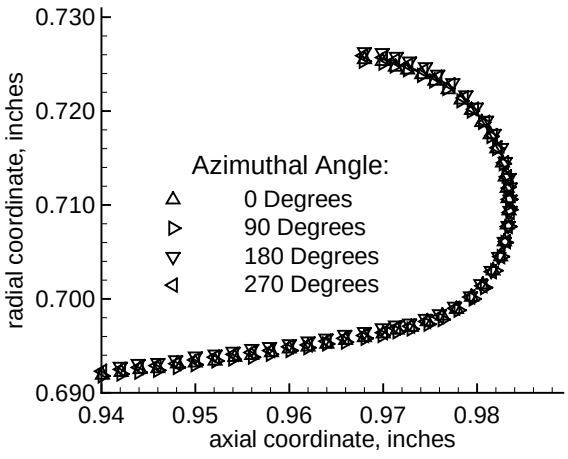

Figure 3: Measured Coordinates of Surrogate Lip

The nickel nozzle was electroformed on a very precise mandrel, and has a very high-quality finish, yet it performs much worse than the surrogate. The investigation almost immediately focused on the tip of the bleed lip.

Computations by ONERA in France have shown that separation can occur on bleed lips for quiet nozzles [17]. It is fairly well known that separation bubbles can lead to early transition downstream, because they are highly unstable [18, 19]. Flat plates used for low-speed transition experiments have carefully designed leading edges in order to avoid separation, and they usually include a trailing-edge flap in order to control the location of the leading-edge stagnation point and therefore the upstream pressure gradients [20]. Rutgers University had already performed computations to show that a separation bubble did occur near the bleed lip [15, 16].

The bleed lips of the nozzle throats were therefore measured in order to check the coordinates. Fig. 3 shows the results for the surrogate lip (here, the axial coordinate is zero at the throat, but the sign is reversed from z, and it increases going upstream). The coordinates appear to be nearly exactly as specified. The nickel nozzle was then measured, as shown in Fig. 4. While the coordinates are generally as designed, there is a 0.001-inch kink near the inner shoulder at the 90-deg. azimuth (and also, to a lesser extent, near the 270-deg. azimuth). This kink is the only known feature in which the nickel nozzle is inferior to the surrogate, so it appears to account for the difference in performance.

This kink aggravates the problem with separation near the lip, and apparently causes the early nozzle-wall transition at 8 psia. The lip of the nickel nozzle

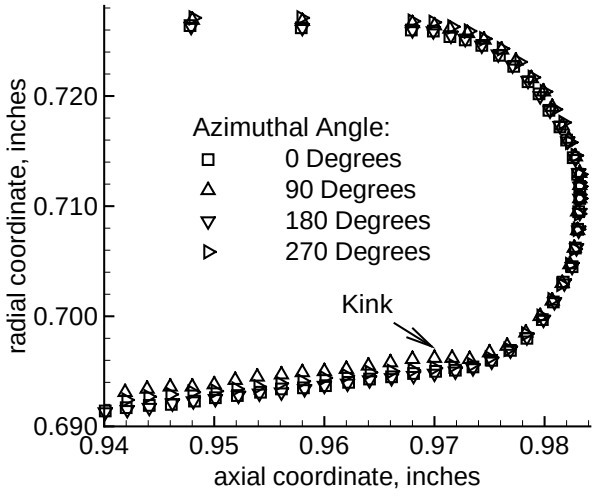

Figure 4: Measured Coordinates of Electroformed Lip

Figure 5: Polished throat with nicks on bleed lip at 7 o'clock

had not been measured previously, due to concerns about damaging the 1-microinch-RMS mirror finish. Figs. 3 and 4 of Ref. [21] show measurements obtained by the manufacturer in the throat of the nickel nozzle, but these measurements did not extend to the lip contour. Ref. [21] does show that the electroform distorted about 0.002 inches out of round when it was removed from the mandrel (about 0.1%). Although detailed records no longer exist for the subsequent machining process (private communication, Larry DeMeno, Allied Aerospace, July 2005), it appears that the electroform was aligned in the lathe as though it was axisymmetric, before the tip and upper surface of the bleed lip were machined. The flaw which was then machined into the lip was not detected due to concerns about damaging the surface finish. In hindsight, these concerns were excessive and unwarranted, since a high-quality measurement need not damage the finish anyway.

The next change made to the surrogate was to have it polished by Optek, Inc. This high-quality polish made a dramatic improvement in the internal finish. Unfortunately, the bleed lip was also nicked, probably during installation, as shown in Fig. 5. The nozzle was then quiet only to about 12 psia., about 1/3 of the previously observed value, and the nick was the obvious possible cause. Mr. Jerry Hahn then hand-polished the nozzle, to reduce the nick, which improved its quiet-flow performance to 34 psia stagnation pressure. This was better, but still lower than before the polish, presumably due to the residual effect of the nick.

High Reynolds-Number Quiet Flow with the Surrogate Throat

The surrogate throat was then repolished by Optek, who concentrated their work near the throat, and extended the polished region around the bleed lip. The nozzle was returned and installed (uneventfully) for tests in late September, 2005. The nozzle flow was measured using a fast Kulite pressure transducer operated as a pitot-pressure sensor. The sensor was placed on the centerline at $z = 45.0$ inches and also $z = 93.4$ inches, for initial driver-tube pressures ranging from 40 to 121 psia. A typical test yielded pressure traces similar to Fig. 6.

Here, the first second of data is from before the run, and provides a baseline. The double-diaphragm breaks near time $t = 0$ seconds, triggering the Tektronix TDS7104 digital oscilloscope, operating in Hi-Res mode at 200 kHz. The pitot pressure is shown in blue, and the wall pressure at the contraction entrance is shown in green. The contraction-wall pressure is essentially the stagnation pressure, since the Mach number in the driver tube is about 0.003. It drops in small stairsteps when the expansion wave reflects from the contraction entrance, about every 0.2 seconds. In Figure 6, the flow was noisy until about 3.3 seconds, when the pitot fluctuation level drops dramatically, indicating that the nozzle-wall boundary layers at the acoustic origin have dropped laminar. A calibrated trace of the contraction pressure indicates

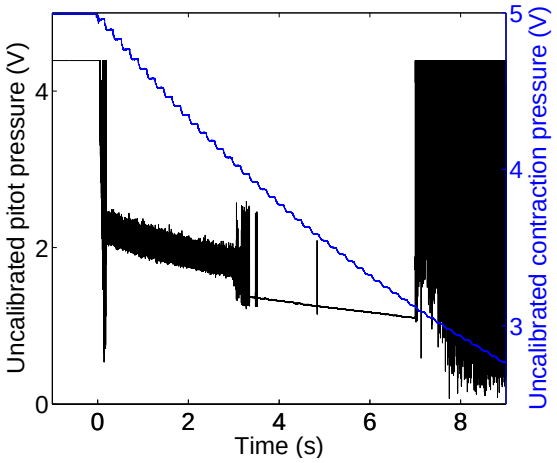

Figure 6: Typical voltage traces for pitot and contraction-wall pressure sensors

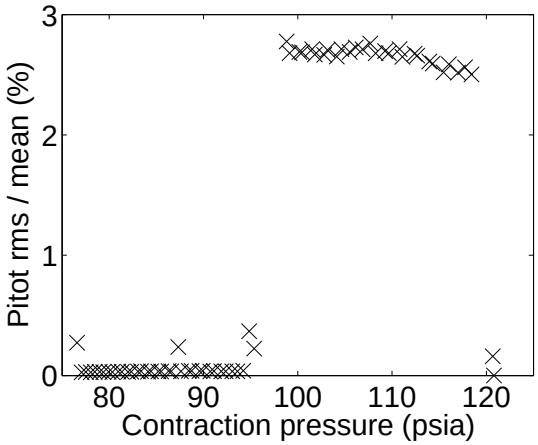

Figure 7: Typical drop from noisy to quiet for a single run starting at 120 psia

that the flow dropped quiet at about 95 psia. The flow is quiet until t = 7 seconds except for turbulent bursts at 3.5 and 4.9 seconds. The run is over at $t = 7$ seconds, when the flow drops subsonic.

The raw traces are analyzed by finding the mean and RMS pressure over short intervals as the stagnation pressure drops in the driver tube. A sample of the short-time-averaged trace is shown in Fig. 7. The traces for early times at higher contraction pressures show high rms noise, which drops suddenly when the contraction-wall pressure drops to about 95 psia. At lower pressures, the quiet flow is generally very quiet, with an rms pitot pressure less than 0.05% of the mean. However, most runs still have two to eight extremely short duration spikes of higher pressure. These are probably turbulent bursts.

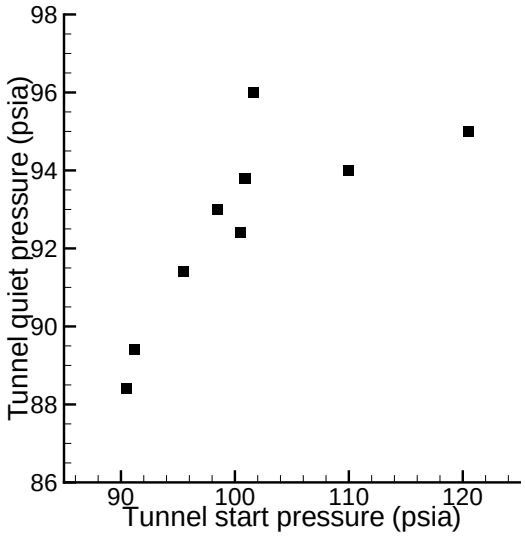

Figure 8: Dependence of tunnel quiet pressure on run start pressure

Experiments were performed at various initial pressures, to see if the stagnation pressure at which the tunnel dropped quiet depended on the time during the run at which that pressure occurred. The results are shown in Fig. 8. Tests begun with a driver tube pressure less than 92 psia were quiet after the startup disturbance. Tests begun at driver-tube pressures from 95 to 121 psia ran noisily until the pressure dropped to about 94 psia, then became quiet. All runs were with a $160°C$ driver tube temperature.

Quiet pressures from a pitot mounted halfway up the nozzle, at $z = 45.0$ inches, agree well with results from the short pitot, at $z = 93.4$ inches; the flow drops quiet at about the same pressure. This correspondence suggests that a bypass mechanism at the bleed lip is still responsible for transition, as in earlier measurements [22]. It seems likely that a separation bubble on the bleed lip is still causing transition, only not as early as it does when the bubble is aggravated by the kink in the nickel lip.

Finally, the Mach number was calculated from the Rayleigh pitot formula, as shown in Figure 9. There is a marked increase in Mach number when the flow becomes quiet. This is expected, since the laminar boundary layer is thinner, and so the area ratio from the throat is larger. This same step in the mean pitot pressure when the flow drops quiet can also be seen in Figure 6.

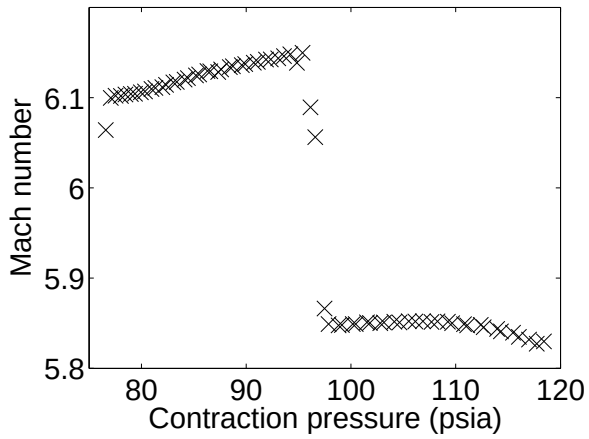

Figure 9: Dependence of Mach number on pressure during a run; same run as previous Figure

Future Plans

The next modification to the surrogate is to remachine the bleed lip to the coordinates provided by Professor Knight's group at Rutgers. This new shape is expected to eliminate the separation bubble that apparently still exists there. A similar series of tests will determine the new maximum quiet pressure and whether there is an axial dependence. The current plan is as follows:

1. Measure coordinates of aluminum bleed lip, as polished
2. Machine new bleed-lip shape provided by Rutgers, to eliminate separation, using aluminum surrogate
3. Measure the as-machined shape
4. Measure the performance of the new shape in the tunnel, before polishing
5. Polish the aluminum throat, then measure again
6. If successful, machine the lip of the electroformed nickel throat
7. Measure the as-machined shape
8. Measure the performance of the nickel throat with the new bleed lip shape

Measurements in the Contraction Inlet

Driver-Tube Noise Levels

Until recently, the flow upstream of the throat had not been measured or characterized to determine its role in the early nozzle-wall transition. Noise in the settling chambers of quiet tunnels has been observed to propagate downstream in measurable quantities. It was also thought that sufficiently high noise levels in the flow exiting the driver tube could be a cause of early nozzle-wall transition. These observations underscore the importance of examining the flow exiting the driver tube at the contraction entrance, so as to determine if the disturbance levels are within acceptable limits.

Beckwith et al. concluded that the dominant disturbance mode in the settling chambers of blow-down wind tunnels is in the form of acoustic energy. These acoustic disturbances propagate downstream primarily as plane waves [23].

Of the acoustic disturbances present in settling chambers, it was estimated by Beckwith that somewhere between 20% and 40% of this energy is transmitted into the test section of supersonic tunnels. It was found that empirical results agree well with theory for Mach numbers up to at least 5 and frequencies up to 60 kHz [23, 24]. However, these facilities had much smaller contraction ratios than the BAM6QT, around 88. The contraction of the BAM6QT most likely reflects much more of the noise back into the driver tube, since its contraction-area ratio is approximately 145.

Experiments were carried out to ascertain the effects of transmitted settling chamber noise on test section noise levels and flow characteristics. In supersonic wind-tunnel tests at JPL, it was found that for a free stream Mach number of 1.78, settling chamber turbulence levels had a strong effect on transition Reynolds numbers for models in the test section. No such effect was observed for Mach numbers between 2.55 and 4.5 [25]. This behavior was also observed in independent tests at Mach 5 in a NASA Langley tunnel. A settling chamber noise increase from 0.35% to 0.85% caused no measurable increase in free stream noise levels [26].

Contrary to these findings, it was observed, in an initial examination, that transition on sharp cones in the Langley Mach-8 Variable Density Tunnel was significantly affected by upstream disturbances. Various configurations of upstream valving and screens provided changes in settling chamber noise levels. Furthermore, additional Mach 5 data indicate that RMS

pitot-pressure levels and trends had some dependency on settling chamber screen configuration [27].

Beckwith et al. completed detailed studies of methods for attenuating the observed noise in the settling chambers of supersonic wind tunnels. In a pilot quiet facility at NASA Langley with Mach 5 nozzles, noise levels in the settling chamber were reduced from an unspecified amount to below 1% with the use of "acoustic baffles" and screens. The acoustic baffles consisted of porous Rigimesh plates. About 12 inches of steel wool were then added to the settling chamber. This further reduced the fluctuation levels to about 0.2% [23]. NASA Langley also used such acoustic baffles in the settling chamber of the Supersonic Pilot Tunnel. Though this facility had mass flows nearly an order of magnitude higher than that of the Mach 5 facility, settling-chamber noise was again very effectively reduced [24].

Clearly, it is uncertain what settling chamber noise levels are acceptable. Considering the success NASA Langley has had in the area of operational quiet tunnels, it is inferred that if the driver tube of the BAM6QT has noise levels comparable to those present in the quiet Langley tunnels, they are within an acceptable range. Beckwith suggested that total disturbance levels in the settling chambers of quiet tunnels should be reduced to 1% or less [26]. If this is not found to be the case in the BAM6QT, there are a number of relatively easy and inexpensive components that could possibly be added to attenuate noise levels appreciably. However, these solutions may not work in a Ludwieg tube due to the short run time.

The following summarizes Ref. [28] which should be consulted for additional detail.

Experimental Setup

The driver tube and contraction must be heated to approximately 160°C to avoid nitrogen liquefaction in the nozzle exit. To aid in this uniform heating, the driver tube is insulated with 3 inch fiberglass pipe insulation. The tube is heated by generating a 6V electric potential drop across the length of it. This draws approximately 2000 amps through the driver tube, which is heated via Ohm's-law. A thermocouple near the downstream end of the driver tube is typically used to control the temperature, although which thermocouple is the controlling thermocouple can be changed. Four Electronics Measurement Incorporated TCR10T750 power supplies provide the necessary current for heating. These power supplies have a maximum output of 750 amps at 10 volts and are regulated by an Omega CN9000A controller.

In order to keep the contraction from being a large heat sink that reduces the temperature of the downstream end of the driver tube, three band heaters are used to heat the contraction. A schematic of the contraction and band heaters can be seen in Figure 10. The two upstream heaters are Tempco 1500W, 240V heaters and the smaller downstream heater is a Tempco 3000W, 240V heater. Each heater is controlled by an Athena Controls, Inc., AIM15 controller. Surface thermocouples are affixed to the contraction by hose clamps and are used by the controllers to determine when each heater needs power in order to keep the temperature at the set point.

The three contraction band heaters are typically set to 138, 160, and 160°C, going from the most upstream heater to the most downstream heater. The most upstream heater is always set lower than the other two. It has been found that this enables all three to actually heat the tunnel. Otherwise, the large upstream heater does all the heating. A HEAT 30kW circulation heater, set to 165°C, was used to heat the incoming air. The circulation heater was controlled by a Watlow 988A-10KD-AAGR heater controller. By examining the readout of a thermocouple located near the upstream end of the driver tube, it has been found that the actual temperature of the heater equilibrates to about 5°C lower than its set point.

It is not easy to make measurements in the driver-tube exit or contraction entrance, since both the driver tube and contraction are ASME code-stamped pressure vessels, and not readily modified. However, measurements are possible using two access ports provided at the entrance to the contraction, near the driver tube exit. The access ports are centered 6.500 inches downstream of the beginning of the contraction, where the tunnel radius has only decreased from 8.750 inches in the driver tube to 8.705 inches [29]. The bottom access port has a diameter of 3.000 inches while the top access port has a diameter of 1.000 inch. The locations of the access ports can be seen in Figure 10.

In order to utilize the instrument ports in the top and bottom of the contraction, two traverse mounts were designed and used in the tunnel. The hot-wire positions in the contraction were changed by adjusting the lead screws of the traverses holding the probe supports. A Velmex A2509BE-S2.5 Unislide traverse allowing 6.5 inches of vertical movement and a Velmex A2515BE-S2.5 Unislide traverse allowing 13.0 inches of vertical movement were used to position the hot-wire probes in the contraction. Both traverses are equipped with a Vernier scale allowing positioning to within 0.001 inches.

Both probes were positioned in the probe supports by removing the blanks from the contraction and inserting the appropriate hardware. Thus the distance between the probe and the contraction wall

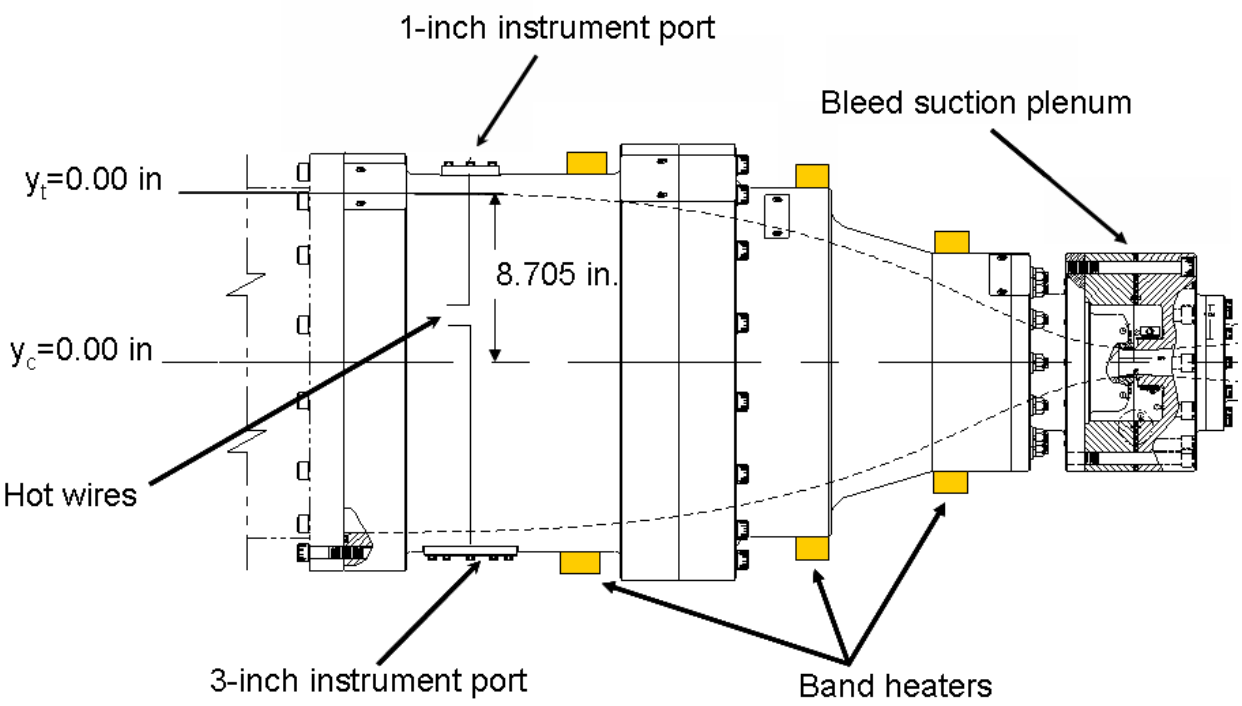

Figure 10: Schematic of the contraction

could be measured using digital calipers. A visual inspection estimates the error in initial probe position to be 0.01 inches. Thus, the precise distance the probe was moved could be readily determined, but the actual position error was set by the initial uncertainty. Two 18-inch TSI 1160-18 high-temperature probe-supports were used to support the probes in the tunnel.

TSI 1222-P12.5 high temperature hot-wire probes were used for both hot-wire and cold-wire investigations. Platinum/10%-Rhodium (Pt/Rh) wires were used for all contraction measurements. They had a diameter of 0.00015 inches and a length/diameter ratio of approximately 340. The probes were inserted into the contraction via the access ports as seen in Figure 10.

When the probe was operated in constant current mode, an in-house constant current anemometer (CCA) was used to power the probe and condition the probe's output signal. Two outputs are available from the anemometer, a DC signal with a gain of 100, and a high-pass filtered AC signal with a gain of 10,000. The high-pass filter is a simple RC filter with a design point of 800 Hz.

For hot-wire applications, a TSI IFA-100 constant temperature anemometer (CTA) was utilized. The CTA was operated using the standard-2 bridge.

Kulite pressure transducers were used to record pressures in a number of tunnel locations. A Kulite model XTEL-190-200A was wall-mounted in the 3-inch port at the entrance to the contraction. A Kulite XT-123CE-190-300SG transducer was used for pressure measurements in the bleed suction plenum. Both of these locations can be seen in Figure 10.

Kulite XCQ-062-15A transducers were used to measure pitot pressure on the tunnel centerline at an axial location of z=75.3 inches (where the nozzle throat is at z=0.0 inches). These transducers were modified by the manufacturer so that the transducer diaphragm was physically stopped above about 15 psia. This allowed high pressure-resolution data to be recorded during a tunnel run, when the pitot pressure is typically less than 2 psia, while protecting the sensor from damage during the substantially higher pre-run pressures. The stock pressure transducers are designed to maintain their calibration for pressures up to twice the design pressure, 15 psia in this case, and to survive only up to three times the design pressure, well below the maximum pressure seen in the tunnel. Additionally, a temperature-sensing wire was added to the output to allow calibration adjustments for variations in the transducer temperature.

In-house electronics were used to power the pressure transducers and condition the output signal. One output was the DC signal with a gain of 100. The other was high-pass filtered at 800Hz with a gain of 10,000, effectively isolating the AC component of the

signal.

Data were recorded on one of four oscilloscopes. A Tektronix TDS7104 digital oscilloscope operating in Hi-Res mode was used to capture all hot and cold-wire data. In Hi-Res mode, the oscilloscope samples data at a rate of 1 GS/sec and then averages it into memory at the set sampling frequency. A Tektronix TDS5034B digital oscilloscope operating in Hi-Res mode was used to capture some static-pressure data in the contraction. For sampling frequencies of 200kS/sec, the Tektronix oscilloscopes in Hi-Res mode gives 15 bit resolution. The oscilloscope can store 4Mb in Hi-Res mode. A LeCroy 9314AL and a LeCroy 9304AM digital oscilloscope were used to record additional data. The 9314AL sampled data at 100kS/second while the 9304AM sampled at 25kS/second. Both gave 8 bit resolution. Only the bleed-slot plenum data were ever recorded on the 9304AM oscilloscope.

A Paroscientific, Inc. Model 740 digital pressure gauge (0-400 psia) was used to monitor the pre-run pressure upstream of the burst diaphragms. It was also used to obtain pressure data for the pressure-transducer calibrations. This quartz-beam gauge is very stable and accurate to 0.01% of full scale.

Free Convection in the Contraction

Initial measurements showed high levels of fluctuations in both the pre-run and the run data. It was hypothesized that free convection due to the non-uniform contraction/driver-tube heating could have been the cause. This possibility was investigated by positioning one hot wire in the nominally stagnant air of the contraction.

For this study, an overheat ratio of 1.62 was used for all data recorded. The driver tube and contraction temperatures were set to 160°C. All oscilloscope traces were recorded with a sampling frequency of 500 kS/s. All y_t distances represent distances below the top contraction wall.

The tunnel was pressurized to approximately 26 psia. Four-second oscilloscope traces were recorded every 10 minutes over a period of 2 hours at y_t=0.10, 0.35, 0.60, 1.10, 1.35 inches, at a sampling rate of 250kS/sec. Traces were also recorded every 10 minutes over an 80 minute period at y_t=0.85 inches. Additionally, traces were recorded over a 30 minute period for y_t=1.50 inches to 6.50 inches below the top tunnel wall, in 0.50 inch increments. All records were thus 1.9Mb long.

Figure 11 shows the RMS plotted against y_t for times of 0, 10, 20, and 30 minutes after the driver tube was pressurized to 26 psia. The average RMS was found by breaking each trace up into segments

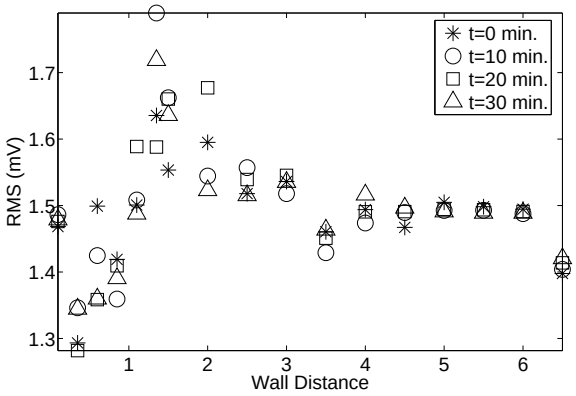

Figure 11: Average RMS vs. y_t

of length 0.02 seconds, finding the RMS of each segment, and then averaging the RMS value of all the segments. Here, the electronic noise was not subtracted. For some voltage traces, the measured noise levels were indistinguishable from the calculated electronic noise, and at times was found to be slightly less than the electronic noise.

No temporal dependence can be seen in Figure 11. Additionally, the average RMS 0.10 inches from the wall is near the RMS levels observed from 3.00 to 6.50 inches from the wall. The average RMS then drops sharply and then increases rapidly to a maximum value around 1.50 inches from the upper contraction wall. The RMS then recovers to a nearly constant lower value between 3.00 and 6.50 inches from the wall.

This behavior was unexpected. It was thought that if a wall effect were causing the observed free convection, the effects would be greatest near the wall and then decrease as distance from the wall increased. This is clearly not the case.

It was thought that an examination of the temperature profile in the contraction would provide an explanation for this unexpected behavior.

Contraction Temperature Measurements

Full-Temperature Contraction

In order to help explain the observed pre-run free convection in the contraction, temperature profiles were measured in the contraction for several different initial stagnation pressures. It is possible that a sufficiently large temperature gradient could have been responsible for the free convection. If such a gradient

also existed in the driver tube, it could have a negative impact on flow quality, introducing undesired disturbances and creating a generally non-uniform flow. These non-uniformities and disturbances could be washed downstream and augment noise levels in the contraction and/or adversely affect the nozzle-wall boundary layer transition.

In order to obtain temperature information in the contraction, the hot wire was operated in constant-current mode. All runs were sampled at 200KS/sec for 10 seconds in Hi-Res mode. Here, the recovery factor was taken to be 1 because of the low Mach number in the contraction.

Due to traverse limitations, the lowest point the wire could reach in the contraction was 3.00 inches below the centerline (although the diameter was 17.41 inches). Measurements were made for locations of y_c=-3.00, -2.00, -1.00, 0.00, 1.00, 2.00, 3.00, 6.00, and 8.00 inches with the tunnel centerline being y_c=0.00 inches. Measurements were made for initial driver-tube pressures of 8, 90, and 145 psia. Locations from y_c=-3.00 to 2.00 inches were measured first for each pressure. The probe support was then moved up on the traverse to allow the wire to reach locations of y_c=3.00, 6.00, and 8.00 inches. For these runs, the driver tube temperature was set to 160°C. The tunnel was filled in the usual manner.

Figure 12 shows the temperature as a function of distance from the centerline in the contraction at an initial driver-tube pressure of 90 psia, for times of -0.5 seconds to 5.5 seconds in 1 second intervals with 0 seconds being the time the run was initiated. Thus, the points corresponding to -0.5 seconds correspond to the pre-run temperature. Each point shows the temperature averaged over 0.25 seconds. Figure 13 shows the temperature as a function of time for an initial driver tube pressure of 90 psia for the aforementioned contraction locations.

As expected, for all values of y_c examined, the temperature dropped with time. This was due to the isentropic expansion of the driver-tube gas from the passing expansion waves.

Unexpectedly, the pre-run temperature at the two locations closest to the upper wall, y_c=6.0 and 8.0 inches (0.705 and 2.705 inches from the top tunnel wall, respectively) were much higher than the set point of 160°C. With a uniformly heated and insulated driver tube, and a uniformly heated contraction, it was expected that the air temperature for all y_c would be very close to 160°C. As can be seen in the figures, the temperature at these locations is the highest for all pre-run data points and decreases slightly with increased initial driver-tube pressure. For locations closer to the tunnel centerline, the pre-run tem-

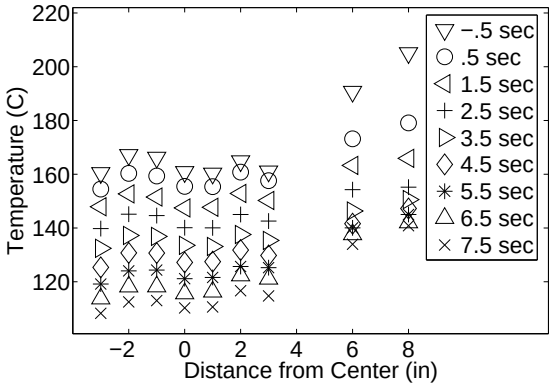

Figure 12: Contraction-air temperature vs. y_c for full-temperature driver tube at an initial pressure of 90 psia

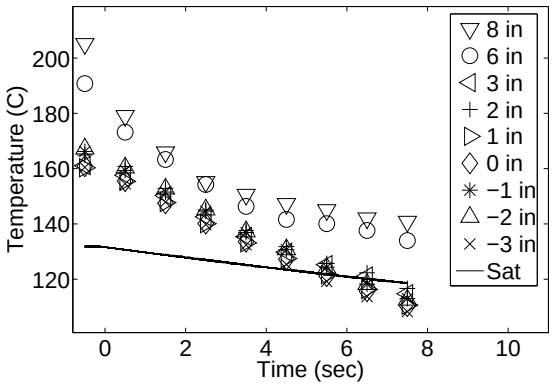

Figure 13: Contraction-air temperature vs. time for full-temperature driver tube at an initial pressure of 90 psia

perature was much closer to the expected value.

For the y_c=6.00 and 8.00 inch cases, the temperature drops off very rapidly after the beginning of the run and approaches a temperature near what was measured at other locations, though the temperature remains consistently higher than those measured at other locations. Due to the rapid temperature drop-off at these locations, it is thought that the high pre-run temperatures are due to overheating of the contraction, not the driver tube. Since measurements were made at the contraction entrance, the pre-run temperature is the only one that reflects the temperature of the air heated in the contraction. Points for temperatures during a run are primarily the temperatures of air heated in the driver tube. After the flow begins, the air in the contraction entrance moves at about 5.5 feet/second. By the time the second data point at 0.5 seconds is calculated, most of the air present in the contraction prior to a run has been evacuated into the nozzle and bleed system and replaced by air from the driver tube.

It was thought that the higher pre-run temperatures near the wall were due to the manner in which the contraction heating was controlled. There are 3 band heaters on the contraction. A J-type thermocouple is attached to the contraction very near each band heater using simple hose clamps. A photograph of one of the thermocouples is shown in Figure 14. The temperature sensed by the thermocouple is used by the band-heater power supply to determine when each heater is in need of power.

The contraction overheating appears to be caused by the outer sides of the controlling thermocouples that were left open to the room air. Heat is transferred from their outer sides into the room, making them read a misleading lower temperature.

It is interesting to note that the temperatures at y_c=6.00 and 8.00 inches are consistently higher than at lower locations. This is evidence that during the equilibrium time between filling the driver tube and running the tunnel the driver tube air stratifies significantly due to temperature variations. If the driver tube walls were well-insulated and uniformly heated, such stratification would not be observed; the air would be at a uniform temperature and no stratification would be observed. It seems that this stratification is caused by the observed pre-run free convection.

Additionally, the theoretical contraction temperature providing static liquefaction of nitrogen in the exit of the nozzle was computed. This curve is seen in Figure 13.

Pope [30] provides the following relation for static nitrogen liquefaction:

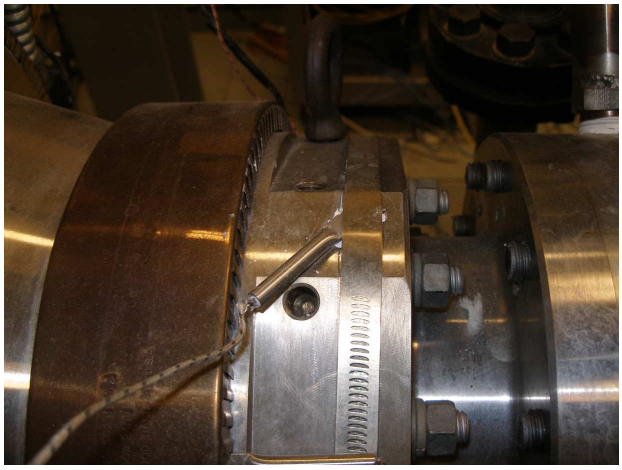

Figure 14: Thermocouple used to control contraction heating

$$\log_{10}(p) = \frac{-605.4}{T} + 4.114 \tag{1}$$

where p is the pressure in atmospheres and T is the static temperature in °R. Since the static pressure in the contraction is the nozzle stagnation pressure, the isentropic static pressure was calculated for a Mach number of 5.8. This gave the static pressure in the nozzle exit. The theoretical static temperature providing nitrogen liquefaction was then calculated. The corresponding stagnation temperature was found via isentropic relations. This is what is plotted as the saturation temperature for nitrogen in the nozzle exit.

As can be seen in Figure 13, there may be some static nitrogen liquefaction in the nozzle exit late into the run. This is an issue that must be addressed later as such liquefaction is undesirable. However, it is possible that supercooling could allow the nitrogen in the air to be cooled below this static-liquefaction point without actually condensing.

Reduced Contraction Temperature

In order to mitigate the effect of overheating the contraction, the band-heater set points were reduced and similar measurements were repeated. The heaters were all turned down to 120°C.

Runs were made at the same initial driver tube pressures and at locations from y_c=-3.00 to 8.00 inches in 1.00 inch increments. The runs were not made in sequence in order to remove any sort of sequence-dependence. Runs were made in two groups and in the following order: -3.00, 2.00, -2.00, 1.00, -1.00, 0.00 (first group) and 3.00, 8.00, 4.00, 7.00, 5.00, 6.00 inches. The first grouping was completed at 8, 90, and 145 psia respectively. The probe support was

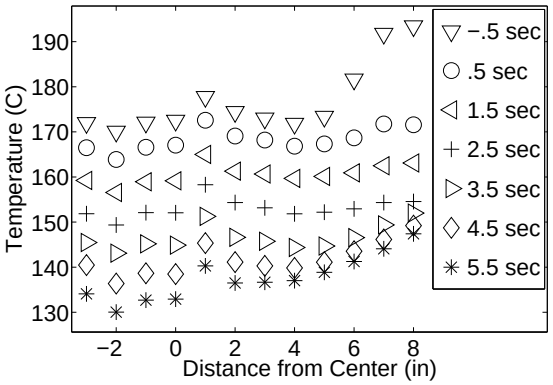

Figure 15: Contraction-air temperature vs. time for reduced-temperature driver tube at an initial pressure of 90 psia

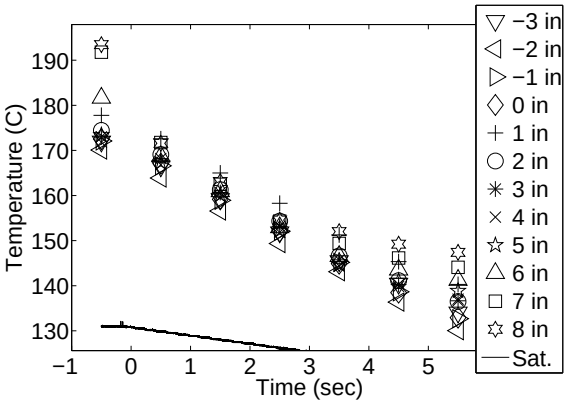

Figure 16: Contraction-air temperature vs. distance from centerline for reduced-temperature driver tube at an initial pressure of 90 psia

then moved up in the traverse to allow the wire to reach the locations in the second grouping. Measurements at the second set of heights were then made for 145, 90, and 8 psia, respectively. Sample results for 90 psia can be seen in Figures 15 and 16.

As can be seen, the pre-run temperatures for locations 6.00 and 8.00 inches above the centerline were lowered by about 10°C. Surprisingly, however, the pre-run temperatures for locations closer to the centerline were approximately 10°C higher than for the fully heated contraction.

The reason for this unanticipated behavior can be explained by the manner in which the driver-tube temperature is controlled. The thermocouple that reads in the driver-tube temperature to the driver-tube controller is located about 3 feet upstream of the contraction. When the contraction temperature is lowered, the downstream end of the driver tube cools as well. The driver-tube temperature controller then finds the driver tube at a lower temperature and increases the driver-tube temperature accordingly. The elevated driver-tube temperature likely raised the air temperature in the contraction as well, even in the pre-run.

The theoretical saturation stagnation temperature for nitrogen in the nozzle exit is again plotted. As can be seen, the static temperature in the nozzle never drops below the static liquefaction limit. Thus, with the reduced contraction-temperature, the likelihood of static nitrogen liquefaction is greatly reduced.

Temperature Drop Compared to Isentropic Theory

A simple theoretical method for predicting the temporal drop of stagnation temperature and pressure in low Mach-number Ludwieg tubes was developed by Schneider, et al. [31]. The pressure drop is modelled as a simple isentropic expansion from a reservoir through a choked nozzle. The massflow is set by the stagnation temperature and pressure.

The massflow was given by

$$V\frac{d\rho_0}{dt} = -A^*\frac{P_0}{\sqrt{RT_0}}c_1, \tag{2}$$

where

$$c_1 = \sqrt{\gamma\left(\frac{2}{\gamma+1}\right)^{\frac{\gamma+1}{\gamma-1}}}, \tag{3}$$

A^* is the nozzle throat area, V is the driver-tube volume, T_0 is the stagnation temperature, P_0 is the stagnation pressure, ρ_0 is the stagnation density, and t is time.

For a perfect and isentropic gas,

$$\frac{P_0}{P_{0,i}} = \left(\frac{\rho_0}{\rho_{0,i}}\right)^{\gamma} \tag{4}$$

where the subscript "i" denotes initial conditions.

Combining these equations with the perfect-gas relation gave the following as a final relationship for the drop in the stagnation-pressure ratio:

$$\frac{P}{P_0} = \left(1 + \frac{\gamma-1}{2}\frac{A^*}{V}\sqrt{RT_{0,i}}tc_1\right)^{\frac{2\gamma}{1-\gamma}} \tag{5}$$

where t is time from the start of the run.

The stagnation-temperature ratio was then easily found from:

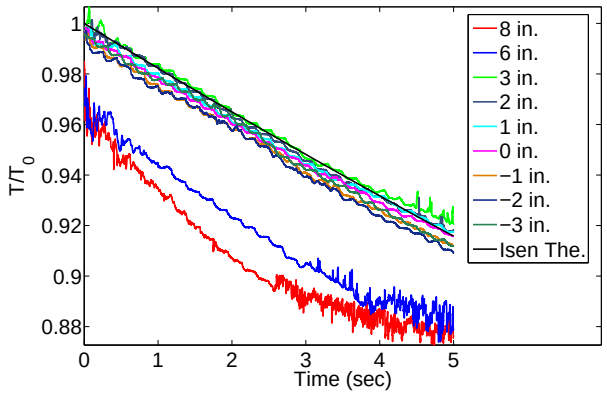

Figure 17: Ratio of stagnation temperature to initial stagnation temperature for 160°C contraction at 90 psia

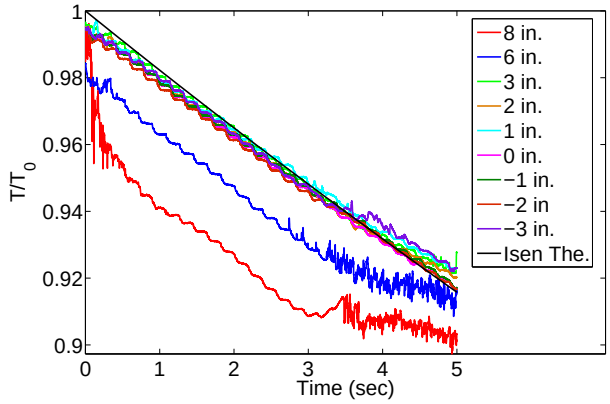

Figure 18: Ratio of stagnation temperature to initial stagnation temperature for 120°C contraction at 90 psia

$$\frac{T}{T_0} = \left(\frac{P}{P_0}\right)^{\frac{\gamma+1}{\gamma-1}} \tag{6}$$

Using these formulas, theoretical temperature ratios were computed and compared to measurements made in the contraction in order to see whether the contraction stagnation temperatures behaved in the same manner as the theory. In each case, T_0 is taken to be the pre-run temperature. Figures 17 and 18 show sample comparisons for the fully heated and the partially heated contraction for an initial stagnation pressure of 90 psia, for y_c=-3.00, -2.00, -1.00, 0.00, 1.00, 2.00, 3.00, 6.00, and 8.00 inches. As can be seen, locations from y_t=-3.00 to 5.00 inches matched very well with the theoretical, isentropic stagnation-temperature drop.

At around 3.5 seconds into the run, however, the actual stagnation temperature begins to turn up slightly. This varies somewhat from the isentropic theory and is possibly due to the growing displacement thickness which effectively reduces the volume of the tunnel, V in Equation 5.

It is clear that there are several locations for which the theory does not come anywhere close to predicting the stagnation-temperature-ratio drop. For the fully heated contraction, wire locations of y_c=6.00 and 8.00 inches showed much lower stagnation temperature ratios for the duration of the runs.

This is most likely due to the high pre-run temperatures observed at y_c=6.00 and 8.00 inches. As was previously discussed, these pre-run temperatures were much higher than the temperatures at those locations just 0.5 seconds into the run. This means that the pre-run temperatures measured at y_c=6.00 and 8.00 inches should not be used as T_0. The appropriate pre-run temperature to use would be the pre-run temperature of the air heated in the driver tube. Unfortunately, this cannot be measured with the current tunnel configuration.

In order to see if a more accurate initial stagnation temperature could be found for air heated in the driver tube prior to a run, various values of T_0 were used in an attempt to bring the experimental temperature-ratio curve closer to the isentropic theory. The values of T_0 that brought the curves close to the theory can be seen in Table 1.

Cont. Temp	T_0 at y_c=8 in	T_0 at y_c=6 in
160°C	177.9°C	175.9°C
120°C	174.9°C	172.9°C

Table 1: Different T_0's used to bring temperature ratios closer to isentropic theory

Figures 19 and 20 show the stagnation-temperature ratio drop with the modified T_0. As can be seen, the curves match the isentropic theory much more closely than in Figures 17 and 18. However, for the cases with the contraction fully heated to 160°C, it is clear that the relationship between the stagnation-temperature ratio and time is characteristically different than the isentropic theory in that it does not have a nearly constant slope. For the 120°C contraction, however, the curves behave much more like the theory.

The differences between theory and the experimental data are thought to be due to a thermal boundary layer present along the upper tunnel wall during a run. This thermal boundary layer is the portion of the fluid near the wall through which the temperature drops from the wall temperature to the free-stream

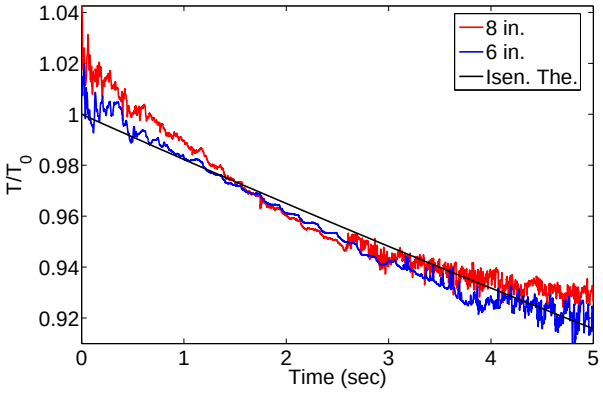

Figure 19: Ratio of stagnation temperature to initial stagnation temperature for 160°C contraction at 90 psia with modified initial stagnation temperature

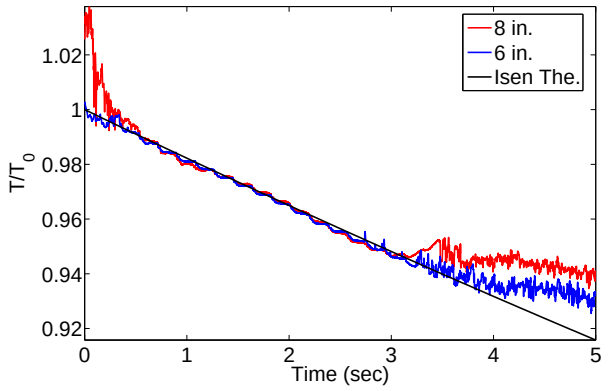

Figure 20: Ratio of stagnation temperature to initial stagnation temperature for 120°C contraction at 90 psia with modified initial stagnation temperature

temperature. Due to the higher contraction-wall temperature, such a thermal boundary layer is expected.

Hot-wire Calibration

Free convection due to the temperature gradient present in the contraction wall and driver tube generates a significantly non-uniform temperature profile in the contraction. This necessitates an examination of the mass-flow fluctuations. The fluctuations present in the driver tube and contraction could significantly affect freestream noise levels in the nozzle or perhaps create a bypass mechanism that trips the nozzle-wall boundary layer.

A calibration of the hot wire was necessary in order to quantify the disturbances in the contraction. Normally, a calibration of a hot wire in low speed, incompressible flow is a trivial task. However, the changing density due to the passing expansion wave in the contraction make this calibration procedure questionable.

A low speed, incompressible hot-wire calibration is normally modelled by King's Law:

$$Nu = A + B\sqrt{Re_w} \tag{7}$$

where A and B are empirical constants, Nu is the Nusselt number, and Re_w is the wire Reynolds number.

The changing density in the contraction, however, makes it unlikely that this relation is accurate. Thus, a new calibration procedure was established and performed. Additionally, the same data were used in another previously established calibration scheme. Mass-flow fluctuations computed from both calibrations were then compared.

For the present study, no contraction boundary-layer effects were considered. As discussed in detail in Ref. [28], the boundary layer in the contraction is highly complex and asymmetric. This makes modelling it in the calibration very difficult. The displacement thickness of the viscous boundary layer would serve to raise the contraction Mach number. It seems likely that a change in Mach number would affect the calibration. No doubt this exclusion added some error and uncertainty to the calibration. However, at present, it seems the only way to proceed.

Calculation of Mass Flow

Both calibration procedures require the mass flow to be known. A simple equation for mass flow is:

$$\rho U = PM\sqrt{\frac{\gamma}{RT}} \tag{8}$$

where ρ is the density, U is the velocity, P is the pressure, M is the Mach number, γ is the ratio of specific heats, R is the gas constant, and T is the temperature.

The contraction-entrance Mach number was found using the isentropic area relationship where the cross-sectional area of the contraction was taken to be 238.1 square inches and the throat area was taken to be 1.7 square inches. This value of the throat area is 1.38 times the geometric throat area to account for the additional area due to bleed-slot suction. Due to the low Mach number, about 0.004, the stagnation and static temperatures are essentially identical at the driver-tube exit. Thus Eq. 8 can be used as an accurate expression for the mass flow.

The static pressure in the contraction, P in Equation 8, was found from the calibrated Kulite static-pressure transducer located on the contraction wall. The sensor was calibrated using the Paroscientific gauge. The tunnel was then pressurized to approximately 145 psia in incremental steps. At each step, the air was allowed to equilibrate and voltage and pressure levels were recorded.

Power-Law Calibration

The goal of this first calibration procedure was to find a relationship between Nusselt number and the wire Reynolds number valid over the entire range of contraction conditions. This could then be compared to the standard King's Law relationship for low-speed incompressible flow. It was thought that the relation would be of the form:

$$Nu = CRe_w^n \tag{9}$$

where C and n are empirical constants determined in the calibration.

The Nusselt number is given by

$$Nu = \frac{E^2 R_w}{\pi k l (T_w - \eta T_0)(R_a + R_w)^2} \tag{10}$$

Due to the low-speed flow, η, the recovery factor, can be taken to be 1 [32]. Here, E is the hot-wire voltage, R_w is the wire resistance, k is the thermal conductivity of air, l is the length of the wire, T_w is the wire temperature, T_0 is the stagnation temperature, R_a is the arm resistance in the constant temperature anemometer, and R_w is the wire resistance.

For calibration purposes, the wire Reynolds number is given by

$$Re_w = \frac{\rho U d}{\mu} \tag{11}$$

where ρU is known from Equation 8.

An analytical expression of the mass flow fluctuations computed from this calibration procedure was found for small fluctuations. The fluctuations can be expressed by:

$$\frac{\widetilde{\rho U}}{\overline{\rho U}} \approx \frac{2}{n} \frac{\widetilde{E}}{\overline{E}} \tag{12}$$

where $\widetilde{\rho U}$ is a fluctuating mass flux, $\overline{\rho U}$ is the mean mass flux, $\widetilde{E}$ is a fluctuating voltage, and $\overline{E}$ is the mean voltage.

Thus the fluctuation levels calculated using this calibration scale with $\frac{1}{n}$. Clearly, the fluctuation levels will be very dependent on the value of n found in fitting the data. The closer n is to 0, the larger the calculated fluctuations will be. Interestingly, the fluctuation levels do not depend on the value C at all.

An additional wire was used to measure the temperature at the hot-wire location. Runs with two wires in the contraction were made for initial stagnation pressures of 8, 15, 25, 35, 45, 65, 90, 105, 125, and 140 psia. These pressures were chosen because over the course of these 6 second runs, almost every pressure between 6 and 140 psia was reached by at least one run. The order in which the initial pressures were run was different than this list, however, in order to remove any sort of dependence on the sequential pressure change. The wire connected to the CTA was positioned on the centerline. The temperature-sensing wire was positioned 0.18 inches below this.

In order to calibrate the wire, the entire run was broken up into smaller periods of length Δt. Each of these periods was used as a data point for finding a calibration relationship for the wire.

The flow temperature was directly sensed by the wire connected to the CCA. The thermal conductivity of the air in the contraction was then calculated from Sutherland's thermal conductivity relation [33]:

$$k = 0.0241 \left(\frac{T}{273} \right)^{\frac{3}{2}} \frac{467}{T + 194} \tag{13}$$

where T is the temperature.

Viscosity was found from Sutherland's viscosity law [33]:

$$\mu = 0.00001716 \left(\left(\frac{T}{273} \right)^{\frac{3}{2}} \frac{384}{T + 111} \right) \tag{14}$$

In both cases, units are MKS. The collected data were used to compute many Nu-Re_w data points. A non-linear least-squares solver in Mathematica was used to fit the data by finding the best C and n of Equation 9 to fit the data.

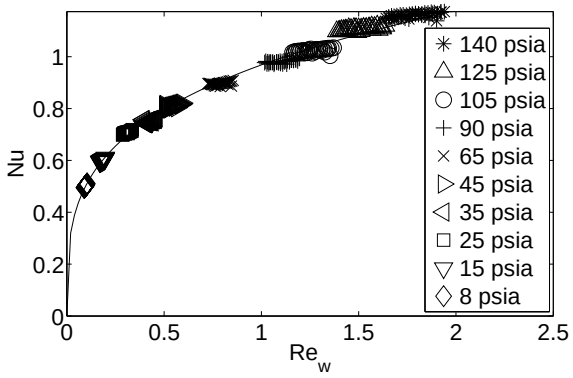

Figure 21: Nu vs. Re_w for the power-law calibration

Figure 21 shows the calibration. Here, the wire Reynolds number is plotted against the Nusselt number. The best fit was found by

$$Nu = 0.970 Re_w^{0.286} \tag{15}$$

As was mentioned before, the mass-flow fluctuations computed from this calibration procedure will scale with $\frac{1}{n}$ (Equation 12). It is essential to examine the change in n for a range of Δt's to ensure that the value of n is not based on this parameter. Additionally, the extent to which the calculated C and n give the best fit of the data must be examined.

The same data shown in Figure 21 were processed for different Δt's. The computed curve-fit parameters are shown in Table 2. As can be seen, for Δt ranging from 0.005 to 0.500 seconds, there is only about a 0.1% change in n. This demonstrates that the value of n is not very dependent on the value of Δt.

Δt	C	n
0.500	0.971786	0.285257
0.200	0.970180	0.285528
0.100	0.970182	0.285529
0.050	0.969938	0.28556
0.020	0.969792	0.285574
0.010	0.969744	0.285579
0.005	0.969721	0.285583

Table 2: Calibration constants calculated for different Δt's

For calculations of mass-flow fluctuations, a Δt of 0.01 seconds was chosen because it gave a reasonable number of data points over which to average. It has been shown that the period of the reflecting expansion wave in the driver tube is approximately 200 ms. If the chosen Δt were too large, many of the aforementioned time periods would include the quasi-static pressure, temperature, and density drop associated with the passing expansion wave. This would skew the mean value for that time period and also introduce a higher RMS. With a Δt of 0.01 seconds, only about 1 in every 20 time periods spanned a passing expansion wave, thus minimizing the effect of the wave.

In order to gain a better understanding of the calibration parameters, it was useful to make a plot in $C - n$ space of how unique the calculated calibration constants were. For a given Δt, Nusselt number and Reynolds number were computed for all calibration data. These values were input into a code which varied C and n over a prescribed range. A correlation coefficient for a linear relationship between the the right and left sides of Equation 9, was calculated. It was found that only one $C - n$ parameter pair fit the data well. This signified that the calibration was unique and trustworthy [28].

Another hot-wire calibration for similar flow conditions was found. The calibration relation is taken from Miley and Horstmann [34, 35] and is as follows:

$$A + B\frac{E^2}{k_f(T_w - T_e)} = Re_f^a \sigma^b \tag{16}$$

where A, B, a, and b are constants found from a non-linear least squares fit of the data, E is the hot-wire voltage, k is the thermal conductivity, T_w is the wire temperature, T_e is the air temperature, Re is Reynolds number based on wire diameter, and σ is the ratio of density of the air to the density of air at sea level. The subscript "f" denotes quantities found at film conditions, defined as the average temperature of the wire and the surrounding fluid.

Miley used this relation to calibrate a hot wire using data collected both in ground facilities and also from a small low-speed airplane flying at different altitudes. The use of airplane data provided an environment of incompressible flow, but with different temperatures and densities. The conditions in the contraction entrance are very similar to this. Miley's data from ground tests and airplane tests collapsed nicely using Equation 16.

This calibration technique was also studied in order to affirm its validity for present experimentation. An analytic analysis of the mass flow fluctuations was again performed to determine the sensitivity to changes in the empirical parameters. It was found that numerous parameter-pairs collapsed the data using this calibration. Thus, it was determined that this calibration procedure was not suitable for the conditions in the contraction of the BAM6QT [28].

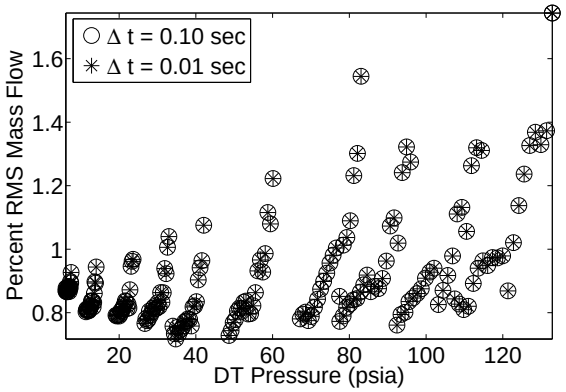

Figure 22: Mass-flow fluctuations on centerline for different Δt during different runs

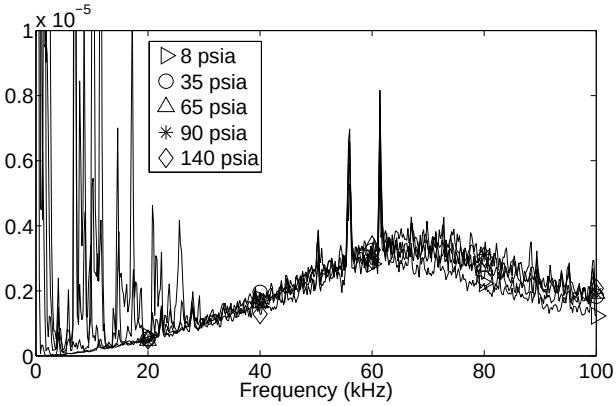

Figure 23: Pre-run power spectra for five pressures

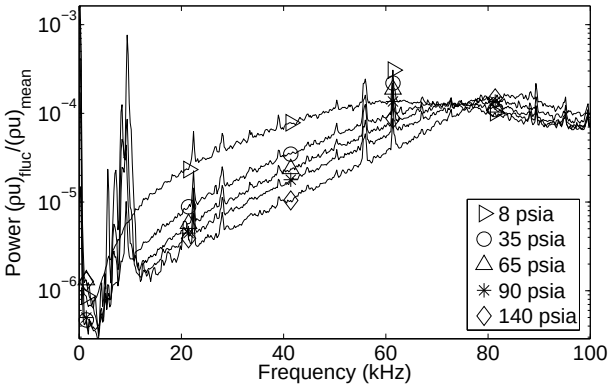

Figure 24: Spectra for run data at five pressures on the centerline

Mass-flow fluctuations

With a calibrated hot wire, the mass-flow fluctuations in the contraction could be easily measured. Mass-flow fluctuation levels were found for y_c=-6.00, -3.00, 0.00, 3.00, and 6.00 inches. As before, data were sampled at 200kHz in Hi-Res mode.

The hot-wire oscilloscope trace from a particular run was converted into mass flow via the calibrations. Both calibrations have a term which is the Reynolds number raised to a power. The Reynolds number was broken up into the mass flow and the quantity $\frac{d}{\mu}$. All quantities other than the mass flow were known. Thus, mass flow was inferred from the Reynolds number for each calibration.

Each run was broken up into periods Δt_{mff}. The RMS for each Δt_{mff} was divided by the mean mass-flow for that period and multiplied by 100 to convert to a percentage.

In order to ascertain the effect on the mass-flow fluctuations of using a different Δt in the calibration procedure, the fluctuation levels were also calculated using the calibration for a Δt of 0.10 seconds. Figure 22 shows fluctuation levels computed for both Δt's. As can be seen, the difference was negligible as it was on the order of 0.03%. The different bands of noise levels correspond to different runs. It is unclear why noise levels are consistently higher at the beginning of each run and then drop off with time.

Figure 23 is the uncalibrated power spectra of the pre-run voltage for pressures of 8, 35, 65, 90, and 140 psia and Figure 24 is the power spectra of the mass flux calculated over the time period from 1.0 seconds to 4.5 seconds. The pre-run spectra is uncalibrated since there is no mass flux in the pre-run and thus applying the calibration to the pre-run voltage would give nonsense mass fluxes. It is still useful, however, to see which frequencies are most prevalent in the nominally stagnant air. In all spectrum plots, $(\rho u)_{fluc}$ represents a fluctuating mass flux and $(\rho u)_{mean}$ represents the mean mass flux.

All power spectra were calculated using the "spectrum" command in MatLab. This subroutine calculates the power spectrum based on the specified number of points per FFT window and the sampling frequency at which the data were collected. In all cases, 1000 points were used for each FFT window. This allowed a frequency resolution of 200 Hz.

Calibrated data were used for all but the pre-run spectra. For each 1000 data points, the mean mass flux was calculated. This was subtracted from the instantaneous mass flux and was then normalized by the mean mass flux. The power spectra were then calculated from this quantity. Most of the differences between the pre-run and run spectra are for the higher frequencies. The peak frequencies increase from about 65kHz in the pre-run to between 65 and 80kHz during the runs.

In Figure 24, the peak frequency shifts by about

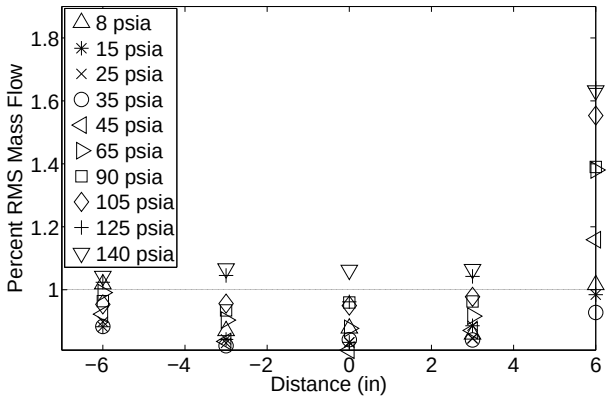

Figure 25: Average fluctuation levels for all locations and pressures examined

10kHz as pressure increases from 8 psia to 140 psia. There are also several large spikes at around 8, 56, and 61 kHz. These are thought to be due to electronic noise since they are present in the pre-run spectra as well. The pre-run spectra also have very large spikes below about 26 kHz. These are most likely due to the observed free convection in the contraction for stagnant air. This explains their absence in Figure 24.

It is curious that during the runs, the majority of the spectral content is found between 60 and 100kHz. This is not the case for the pre-run data, and it is unknown why this is the case.

Noise levels were also found at y_c=-6.00, -3.00, 3.00, and 6.00 inches. In order to present all of the data in one simple figure, the average percent-mass-flow-fluctuation level was calculated for each run. Figure 25 shows these values plotted against y_c. A line is also included showing the 1% level. As can be seen, for y_c=-6.00, -3.00, 0.00, and 3.00 inches, the average fluctuation levels are very similar, ranging from about 0.8% to 1.1%. The fluctuation levels at 6.00 inches are significantly higher, ranging from about 0.95% to nearly 1.7%.

Following Beckwith's criterion of maintaining settling chamber noise levels of less than 1% [26], the fluctuations in the driver tube of the BAM6QT are, on average, marginally too high for y_c=-6.00, -3.00, 0.00, and 3.00 inches. During the course of all of these runs, with the possible exception of runs at 8, 15, and 25 psia, the noise level is greater than 1% for a significant portion of the total run. A more detailed report of the contraction noise levels can be found in Reference [28].

At y_c=6.00 inches, the noise levels are even higher, with only 15 and 35 psia having an average RMS less than 1%. This demonstrates the non-uniformity of the driver-tube noise.

Due to differences between the tunnels used by Beckwith and the BAM6QT, it is possible that the observed noise levels are sufficiently low and do not preclude quiet flow. Beckwith worked with tunnels with much smaller contraction ratios than that of the BAM6QT. For instance, the contraction ratio of the Supersonic Pilot Quiet Tunnel was only about 35, and for the Mach-5 Pilot Tunnel this ratio was about 88 [26]. The BAM6QT has a contraction ratio of about 145. It is conceivable that for a sufficiently large contraction ratio, enough driver-tube noise would be reflected back into the driver tube and not transmitted into the nozzle that driver-tube noise levels of greater than 1% would not affect transition in the nozzle. It is possible that noise levels greater than 1% are acceptable for this facility.

Thus, from these results alone, it is difficult to determine whether the driver-tube noise could be adding to nozzle free-stream noise or affecting transition of the nozzle-wall boundary layer. Further characterization of the fluctuations in the contraction is clearly in order.

Uncalibrated Boundary-Layer Measurements

In order to fully understand the nature of the flow present in the contraction, the boundary layer there cannot be neglected. There has not been a great deal of research into boundary-layer growth in Ludwieg tubes. What has been done seems to apply only to small-diameter Ludwieg tubes with run times on the order of tens or hundreds of milliseconds [36, 37, 38, 39]. This is not the case for the BAM6QT. Additionally, the reflecting expansion wave makes understanding and predicting this boundary layer complicated and difficult. Nevertheless, some precursory work was done to try to understand the nature of the contraction-wall boundary-layer.

Uncalibrated measurements were made near the upper wall of the contraction. At the time of this investigation, the wire calibration procedure had not been established. Additionally, parameters such as Mach number, temperature, and viscosity, since viscosity is a function of temperature, are not the same in the boundary layer. Thus, the current calibration technique would not hold in the boundary layer.

All runs had an initial stagnation pressure of 45 psia. Runs were made for y_t=0.02 to 0.30 inches in 0.025-inch increments. Additional runs were made at y_t=1.02, 2.02, 3.02, 4.02, and 5.02 inches from the upper contraction wall. These distances were chosen because a very simple boundary-layer model predicted a thickness of around 0.1 inches.

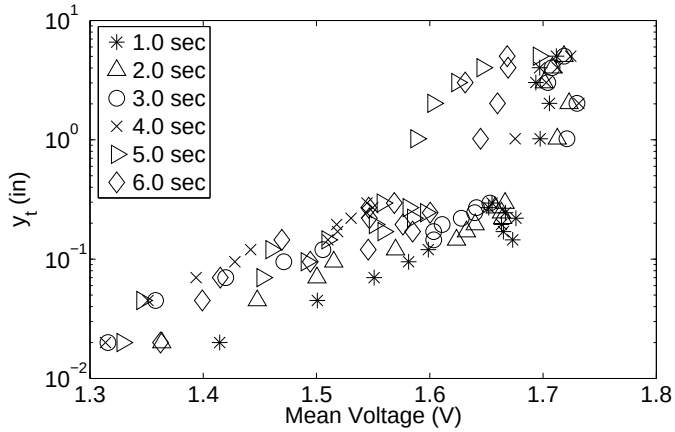

Figure 26: Uncalibrated hot-wire voltage in boundary layer

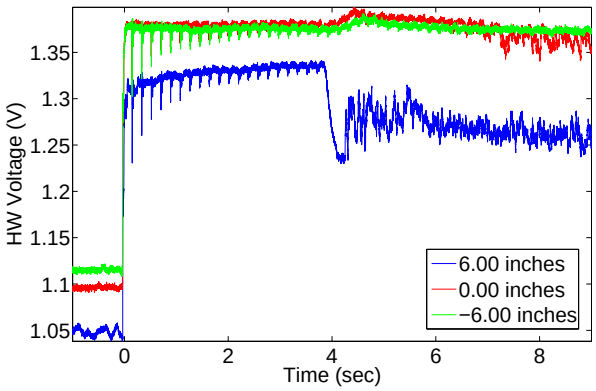

Figure 27: Oscilloscope traces at y_c=6.00, 0.00 and -6.00 inches for 45 psia

As the probe traversed the boundary layer, the mean voltage should have increased until it reached its maximum value in the free stream. Figure 26 shows the results of these runs. Here, y_t is plotted against the mean hot wire voltage, averaged over 0.01 seconds, for 6 different times during the runs.

The figure indicates that the hot-wire voltage generally increased as distance from the wall increased. If the probe were always outside the boundary layer, the mean voltage should be invariant with time. No location ever showed a constant voltage for all times. Instead, each location showed the voltage dropping with time. This would be expected if the probe were in a growing boundary layer. As the boundary layer grew thicker, a fixed y_t location would move further from the boundary-layer edge and thus the mass flux would drop. Since this was the observed behavior, it seems that the probe was in a growing boundary layer at all the y_t locations examined.

It is also of note that for $y_t > 1.0$ inches, the mean voltage at 1.0 second is about the same. However, as y_t was increased from 1.02 to 5.02 inches, the total voltage drop over the run decreased markedly. This indicates that for $y_t > 1.0$ inches, the probe was initially outside the boundary layer but then the boundary layer grew to contain those locations. The data indicate that the upper-wall contraction boundary-layer grows to be at least 5 inches thick by 6.0 seconds into a run at 45 psia.

Qualitative Changes Near the Wall

It was noted that the qualitative nature of the hot-wire oscilloscope traces changed markedly the closer the wire was to the top contraction wall. Figure 27 highlights this difference. Three oscilloscope traces are shown. One was for the wire located on the contraction centerline. The others were located at 6.00 and -6.00 inches. All three are for an initial stagnation pressure of 45 psia. Here, only every 100th point is plotted. As usual, the Tektronix TDS7104 oscilloscope was used and was operated in Hi-Res mode with a sampling frequency of 200kS/s.

The trace on the centerline behaves as would be expected. The data recorded between -1.0 and 0.0 seconds corresponds to pre-run data. The large jump in voltage at 0 seconds corresponds to the startup of the tunnel. There is a slight bump in the trace at around 4.5 seconds after which point the voltage begins to decrease until the end of the run. The trace at y_c=-6.00 inches is almost indistinguishable from that of the centerline. The trace for the wire at y_c=6.00 inches behaves very differently. At about 4.0 seconds, there is a sharp, dramatic decrease in voltage followed by a slight recovery and then high noise until the end of the run. Also, the voltage spikes due to the reflecting expansion wave are no longer discernible. These spikes are periodic and visible at approximately 200 millisecond intervals. This sort of behavior was present in varying degrees for different pressures.

It is thought that the large, sudden voltage drop for the oscilloscope trace corresponding to the hot wire at y_c=6.00 inches is due to the wire's inclusion in the boundary layer. Hot-wire voltage drops with decreased mass flow. The decreased mass flow in the boundary layer would cause such a drop in voltage.

It is of note that this behavior is not seen for the oscilloscope trace corresponding to a wire location of y_c=-6.00 inches. This implies that the probe is never in the lower contraction-wall boundary-layer, even though it is the same distance from the wall as the traces that appear to be in the upper-wall boundary layer. Some boundary layer thickening is expected along the top wall because of the previously

seen stratification in the driver tube in the pre-run. The stratification makes the initial conditions along the upper wall different than those along the bottom wall. This seems to cause quite a dramatic asymmetry in the boundary layer, if that indeed is the cause of the oscilloscope-trace deformities noted at all pressures 6.00 inches above the centerline.

The data here indicate that a more thorough investigation of the contraction-wall boundary layer is in order. This would help resolve the present uncertainties. It is clear, however, that there are large asymmetries in the flow in the contraction. These asymmetries could easily introduce unwanted disturbances and asymmetries in the nozzle flow further downstream. In order to mitigate these disturbances, they must first be properly understood through more experimental work.

Plans for Future Work

To address some of the unresolved issues, the following procedures should be carried out in the contraction of the BAM6QT.

1. Insert a plug into the nozzle throat to see if this mitigates free convection effects
2. Vary contraction and driver-tube temperatures to obtain a more uniform temperature profile
3. Use a hot wire with a different aspect ratio to confirm noise levels
4. Investigate the boundary layer and its effects more thoroughly and, if possible, include them in the calibration procedure
5. Make measurements further upstream in the driver tube and compare
6. Introduce disturbances of known spectral content into the end of the driver tube and determine the percent of the disturbance that is transmitted into the test section
7. If possible, employ some of Beckwith's techniques to mitigate driver tube noise

Summary

Purdue continues to develop the Boeing/AFOSR Mach-6 Quiet tunnel. Recent modifications to the surrogate aluminum nozzle throat yielded repeatable quiet flow to approximately 94 psia. A 0.001 inch kink in the bleed lip was apparently responsible for the low-Reynolds number transition observed in the electroformed throat.

The current study has greatly expanded knowledge of the flow in the contraction entrance of the BAM6QT and has also served to highlight areas in which further study is necessary. Several aspects of the contraction were examined in order to characterize the condition of the flow there.

Free convection in the nominally stagnant pre-run air was found to be a source of significant disturbances. This free convection is thought to have been caused by the large temperature gradient that is present over the length of the contraction wall. The gradient led to non-uniform temperatures in the contraction, which induced the free-convection currents.

The temperatures in the contraction above the centerline, during the pre-run and also during the run, were found to be significantly higher than those on the centerline. After the beginning of the run, the temperatures at that location remained higher than on the centerline, but the difference was much smaller, only about 15°C.

This shows that the contraction wall is actually much hotter than the set point of 160°C, even though the driver-tube walls are near the set point. The contraction overheating appears to be caused by the outer sides of the controlling thermocouples that were left open to the room air. Heat is transferred from their outer sides into the room, making them read a misleading lower temperature. Modifying the contraction band-heater set-points did lower the observed temperature in the contraction, but the perfect settings were not found to make a uniform 160°C temperature profile.

The ratio of the time-dependent stagnation temperature to the initial stagnation temperature was also computed for a variety of pressures and y_c stations. These data were compared to a simple isentropic theory for the drop in stagnation-temperature ratio. For most of the locations and pressures studied, the data matched the theory well. However, for y_c=6.00 and, in some cases, 3.00 inches, the theory overpredicted the drop. It is thought that the higher pre-run temperatures present near the upper contraction wall are mostly responsible for the deviation from theory. However, the slopes of the curves still often did not match the theoretical slope. This is thought to be due to a thick thermal boundary layer on the upper contraction wall during a run caused by the excessively heated contraction walls and also the stratification of the air in the driver tube prior to a run. This thermal boundary layer appears to be asymmetric due to pre-run stratification of the air in the driver tube and was observed to be much thinner along the bottom wall because it was not observed at y_c=-6.00 or -3.00 inches.

Two methods were used to calibrate hot wires in

the incompressible, varying density flow of the contraction. It was found that the established method of Miley and Horstmann is not suitable for the conditions of this experiment. Another calibration method was found that avoided the shortcomings of the Miley method. The Nusselt number was related to the wire Reynolds number via a power-law relationship. It was found that there was only one unique power fit of the data. This led to a stable and trustworthy calibration.

Mass-flow fluctuations were found for many pressures at many y_c locations using this calibration. The levels at all but the 6.00 inch locations are marginally too high according to Beckwith's criterion. At 6.00 inches, they are definitely too high. However, the BAM6QT has now been demonstrated to run quietly to about 95 psia. Thus, driver-tube noise cannot be held responsible for the previous early nozzle-wall boundary-layer transition. It is still possible, however, that the current noise levels will preclude quiet flow to higher stagnation pressures. The fluctuation levels in the driver tube cannot yet be considered low enough to not threaten future quiet-flow development. Additional work is clearly in order.

A precursory examination of the contraction-entrance boundary-layer was also undertaken. Initial measurements at 45 psia showed a boundary layer thickness of at least 5 inches by the end of a run at an initial stagnation pressure of 45 psia. This preliminary data were substantiated by examining a qualitative change between a hot-wire voltage trace on the centerline and one at $y_c = 6.00$ inches. None of this was evident for hot-wire traces taken at y_c=-6.00 inches, suggesting an asymmetric contraction-wall boundary layer. Further work is clearly in order in this area as well.

Acknowledgements

The research is funded by AFOSR under grant F49620-03-1-0030, and by Sandia National Laboratory under contract 80377. Frank Chen and Steve Wilkinson from NASA Langley continued to provide occasional assistance in making the best possible use of information available from the earlier NASA Langley quiet-tunnel development effort. Mr. Gerald Hahn of the AAE machine shop machined the surrogate throat section, and Optek Technologies of Batavia, Illinois provided the high-quality polish. The lip was measured by Anderson Tool of Anderson, Indiana. Prof. Garry Brown of Princeton University suggested the use of a surrogate nozzle throat. Prof. Eli Reshotko drew our attention to Ref. [19]. Larry DeMeno from Allied Aerospace provided expert leadership in the development of the nozzle. Prof. Schneider accepts full responsibility for the 1998 decision not to measure the coordinates of the nickel bleed lip.

References

[1] Steven P. Schneider. Laminar-turbulent transition on reentry capsules and planetary probes. Paper 2005-4763, AIAA, June 2005.

[2] Steven P. Schneider. Hypersonic laminar-turbulent transition on circular cones and scramjet forebodies. *Progress in Aerospace Sciences*, 40(1-2):1–50, 2004.

[3] I.E. Beckwith and C.G. Miller III. Aerothermodynamics and transition in high-speed wind tunnels at NASA Langley. *Annual Review of Fluid Mechanics*, 22:419–439, 1990.

[4] Steven P. Schneider. Effects of high-speed tunnel noise on laminar-turbulent transition. *Journal of Spacecraft and Rockets*, 38(3):323–333, May–June 2001.

[5] Steven P. Schneider. Flight data for boundary-layer transition at hypersonic and supersonic speeds. *Journal of Spacecraft and Rockets*, 36(1):8–20, 1999.

[6] S. P. Wilkinson, S. G. Anders, and F.-J. Chen. Status of Langley quiet flow facility developments. Paper 94-2498, AIAA, June 1994.

[7] I. Beckwith, T. Creel, F. Chen, and J. Kendall. Freestream noise and transition measurements on a cone in a Mach-3.5 pilot low-disturbance tunnel. Technical Paper 2180, NASA, September 1983.

[8] Alan E. Blanchard, Jason T. Lachowicz, and Stephen P. Wilkinson. NASA Langley Mach 6 quiet wind-tunnel performance. *AIAA Journal*, 35(1):23–28, January 1997.

[9] S. P. Schneider and C. E. Haven. Quiet-flow Ludwieg tube for high-speed transition research. *AIAA Journal*, 33(4):688–693, April 1995.

[10] Steven P. Schneider. Design of a Mach-6 quiet-flow wind-tunnel nozzle using the e**N method for transition estimation. Paper 98-0547, AIAA, January 1998.

[11] Steven P. Schneider, Shin Matsumura, Shann Rufer, Craig Skoch, and Erick Swanson. Progress in the operation of the Boeing/AFOSR Mach-6 quiet tunnel. Paper 2002-3033, AIAA, June 2002.

[12] Steven P. Schneider, Craig Skoch, Shann Rufer, Erick Swanson, and Matthew P. Borg. Laminar-turbulent transition research in the Boeing/AFOSR Mach-6 quiet tunnel. Paper 2005-0888, AIAA, January 2005.

[13] Craig Skoch, Steven P. Schneider, and Matthew P. Borg. Disturbances from shock/boundary-layer interactions affecting upstream hypersonic flow. Paper 2005-4897, AIAA, June 2005.

[14] Shann J. Rufer and Steven P. Schneider. Hot-wire measurements of instability waves on a blune cone at Mach 6. Paper 2005-5137, AIAA, June 2005.

[15] Ezgi S. Taskinoglu, Doyle D. Knight, and Steven P. Schneider. A numerical analysis for the bleed slot design of the Purdue Mach-6 wind tunnel. Paper 2005-0901, AIAA, January 2005.

[16] Selin Aradag, Doyle D. Knight, and Steven P. Schneider. Simulations of the Boeing/AFOSR Mach-6 wind tunnel. Paper 2006-1434, AIAA, January 2006.

[17] R. Benay and B. Chanetz. Design of a boundary layer suction device for a supersonic quiet tunnel by numerical simulation. *Aerospace Science and Technology*, 8:255–271, 2004.

[18] Laura Pauley, Parviz Moin, and William Reynolds. The instability of two-dimensional laminar separation. In *Low Reynolds Number Aerodynamics*, pages 82–92, Berlin, 1989. Springer-Verlag.

[19] P. Klebanoff and K. Tidstrom. Two-dimensional roughness element induces boundary-layer transition. *Physics of Fluids*, 15(7):1173–1188, 1972.

[20] Steven P. Schneider. *Effects of Controlled Three-Dimensional Perturbations on Boundary Layer Transition*. PhD thesis, Graduate Aeronautical Laboratories, California Institute of Technology, March 1989. DTIC citation ADA215080.

[21] Steven P. Schneider and Craig Skoch. Mean flow and noise measurements in the Purdue Mach-6 quiet-flow Ludwieg tube. Paper 2001-2778, AIAA, June 2001.

[22] Steven P. Schneider, Craig Skoch, Shann Rufer, and Erick Swanson. Hypersonic transition research in the Boeing/AFOSR Mach-6 quiet tunnel. Paper 2003-3450, AIAA, June 2003.

[23] Ivan E. Beckwith, F.-J. Chen, and T.R. Creel Jr. Design requirements for the NASA Langley supersonic low-disturbance wind tunnel. Paper 86-0763, AIAA, March 1986.

[24] Ivan E. Beckwith and E. Wayne Martin. Propagation of settling chamber noise in supersonic wind tunnels. Presented at the 57th semiannual meeting of the Supersonic Tunnel Association, March 1982.

[25] John Laufer and Jack E. Marte. Results and a critical discussion of transition-Reynolds-number measurements on insulated cones and flat plates in supersonic wind tunnels. Technical Report 20-96, Jet Propulsion Laboratory, November 1956.

[26] Ivan E. Beckwith. Comments on settling chamber design for quiet, blowdown wind tunnels. NASA Technical Memorandum 81948, March 1981.

[27] Ivan E. Beckwith and P. Calvin Stainback. Transition research and prospects for a Mach 3 to 7 quiet tunnel. Langley Working Paper 1064, July 1972.

[28] Matthew P. Borg. Characteristics of the contraction of the Boeing/AFOSR Mach-6 quiet tunnel. Master's thesis, Purdue University, December 2005. Submitted to DTIC.

[29] Steven P. Schneider, Craig Skoch, Shann Rufer, Erick Swanson, and Matt Borg. Bypass transition on the nozzle wall of the Boeing/AFOSR Mach-6 quiet tunnel. Paper 2004-0250, AIAA, January 2004.

[30] Alan Pope and Kennith L. Goin. *High-speed wind tunnel testing*. Robert E. Krieger Publishing Company, 1978.

[31] Steven P. Schneider, Steven H. Collicott, J. D. Schmisseur, Dale Ladoon, Laura A. Randall, Scott E. Munro, and T. R. Salyer. Laminar-turbulent transition research in the Purdue Mach-4 Quiet-Flow Ludwieg Tube. Paper 96-2191, AIAA, June 1996.

[32] E.F. Spina and C.B. McGinley. Constant-temperature anemometry in hypersonic flow: critical issues and sample results. *Experiments in Fluids*, 17:365–374, 1994.

[33] Frank M. White. *Viscious Fluid Flow*, pages 27–31. McGraw-Hill, 2nd edition. Madison, WI, 1991.

[34] S. J. Miley and Dr. Ing. K. H. Horstmann. Data report of flight and wind-tunnel investigations of Tollmien-Schlichting waves on an aircraft wing. Technical Report IB 129-91/18, Institut fur Entwurfsaerodynamik, DLR, December 1991.

[35] Eds. D. Fisher, K.H. Horstmann, and H. Riedle. Flight test measurement techniques for laminar flow. AGARDograph 300, Research and Technology Organisation, October 2003.

[36] E. Becker. Unsteady boundary layers behind compression shocks and expansion waves. *Progress in Aeronautical Sciences*, 1:104–173, 1961. Translated from German to English by Associated Technical Services, Glen Ridge, NJ, 1969.

[37] Chung-Hwan Chun and Taesung Ha. Investigation of the unsteady boundary layer development in a Ludwieg tube. Unpublished report from the Department of Mechanical Engineering, Pohang University of Science and Technology, Republic of Korea. Emailed on 2 June, 2005 by Ch.-H. Chun.

[38] Eckart Piltz. Boundary-layer effects on pressure variations in Ludwieg tubes. *AIAA Journal*, 10(8):1095–1097, 1972.

[39] David A. Russell, Gerald S. Knoke, and John C. Wai. Uniformity of Ludwieg tube flows. From Modern Developments in Shock Tube Research 10th Annual International Shock Tube Symposium, Kyoto, 1975. p. 244-251.